Action of AA9 lytic polysaccharide monooxygenase enzymes on different cellulose allomorphs

Margaux Grellier, Céline Moreau, Johnny Beaugrand, Sacha Grisel, Jean-guy Berrin, Bernard Cathala, Ana Villares

Action of AA9 lytic polysaccharide monooxygenase enzymes on different cellulose allomorphs

Margaux Grellier, Céline Moreau, Johnny Beaugrand, Sacha Grisel, Jean-Guy Berrin, Bernard Cathala, Ana Villares

PII: S0141-8130(24)04234-X

DOI: https://doi.org/10.1016/j.ijbiomac.2024.133429

Reference: BIOMAC 133429

To appear in: *International Journal of Biological Macromolecules*

Received date: 15 April 2024

Revised date: 4 June 2024

Accepted date: 24 June 2024

Please cite this article as: M. Grellier, C. Moreau, J. Beaugrand, et al., Action of AA9 lytic polysaccharide monooxygenase enzymes on different cellulose allomorphs, *International Journal of Biological Macromolecules* (2023), https://doi.org/10.1016/j.ijbiomac.2024.133429

Action of AA9 lytic polysaccharide monooxygenase enzymes on different cellulose allomorphs

Margaux Grellier[1], Céline Moreau[1], Johnny Beaugrand[1], Sacha Grisel [2,3], Jean-Guy Berrin[2,3], Bernard Cathala[1], Ana Villares[1]*

[1] UR1268 BIA, INRAE, F-44316 Nantes, France

[2] INRAE, Aix Marseille Univ., UMR BBF, F-13009 Marseille, France

[3] INRAE, Aix Marseille Univ., 3PE platform, F-13009 Marseille, France

ABSTRACT

Lytic polysaccharide monooxygenase (LPMO)-catalyzed oxidative processes play a major role in natural biomass conversion. Despite their oxidative cleavage at the surface of polysaccharides, understanding of their mode of action, and the impact of structural patterns of the cellulose fiber on LPMO activity is still not fully understood. In this work, we investigated the action of two different LPMOs from *Podospora anserina* on celluloses showing different structural patterns. For this purpose, we prepared cellulose II and cellulose III allomorphs from cellulose I cotton linters, as well as amorphous cellulose. LPMO action was monitored in terms of surface morphology, molar mass changes and monosaccharide profile. Both *Pa*LPMO9E and *Pa*LPMO9H were active on the different cellulose allomorphs (I, II and III), and on amorphous cellulose (PASC) whereas they displayed a different behavior, with a higher molar mass decrease observed for cellulose I. Overall, the pretreatment with LPMO enzymes clearly increased the accessibility of all types of cellulose, which was quantified by the higher carboxylate content after carboxymethylation reaction on LPMO-pretreated celluloses. This work gives more insight into the action of LPMOs as a tool for deconstructing lignocellulosic biomass to obtain new bio-based building blocks.

Keywords: LPMO, cellulose allomorphs, molar mass, carboxymethylation.

1. Introduction

Cellulose degradation has attracted much interest for the development of bioproducts, including biofuels [1], platform chemicals [2, 3] and nanocelluloses [4, 5] for different applications in the fields of composites, packaging or formulations. The major bottleneck of cellulose fractionation is its inherent recalcitrance, arising from the structural complexity leading to crystalline arrangement, necessitating the addition of pretreatments including chemical, mechanical and/or enzymatic methods. While humankind tries to overcome biomass recalcitrance in a sustainable way, nature has already set it up by a battery of enzymes evolved by microorganisms for cell wall degradation. In this context, fungi are the most effective decayers of lignocellulosic biomass, secreting different kinds of enzymes, whose synergistic activity achieves cellulose degradation. Among these enzymes, lytic polysaccharide monooxygenases (LPMOs) can oxidatively cleave polysaccharides. LPMOs are copper-dependent enzymes classified into eight families, AA9-AA11 and AA13-AA17, in the CAZy classification (Carbohydrate Active enZymes database, www.cazy.org) [6-8]. Different AA9 LPMO enzymes are encoded by the genome of the coprophilous fungus *Podospora anserina*, and some of them have demonstrated activity on cellulose, hemicelluloses and cello-oligosaccharides [9-11]. In previous studies, we have shown that these LPMOs can create nicking points that facilitate the fiber deconstruction and further fibrillation [4, 5] and can also attack the tension regions of the cellulose fiber, releasing the tension and increasing swelling and accessibility [12].

Despite the recent breakthroughs in the field, more research is still needed to better understand the mode of action of LPMOs on different cellulosic structural and crystalline patterns. Native cellulose exists as the specific lattice cellulose I (Cell-I), in a two chain monoclinic cellulose I_β phase, with a parallel chain arrangement [13]. The structure is stabilized by intramolecular hydrogen bonds (O3H-O5’ and O2H-O6’), as well as

intermolecular hydrogen bonds between different chains (O6H-O3'') [14]. When cellulose is submitted to different treatments, the chain arrangement is disrupted and different crystalline allomorphs can be obtained. Immersion in sodium hydroxide solutions facilitates swelling as the Na^+ cations penetrate the intracrystalline spaces. As a result, cellulose I is transformed into cellulose II (Cell-II). Cellulose II is a two chain monoclinic allomorph, and presents an antiparallel arrangement of cellulose chains with a new intermolecular hydrogen bonding pattern (O6H-O2'' and O2H-O2'') [14]. When cellulose is treated with amines, such as the ethylenediamine (EDA), the fibers become inflated as the amine molecules penetrate the crystalline areas, and the unit cell is altered to a less dense and metastable allomorph named cellulose III (Cell-III). Hydrogen bonds between cellulose chains are broken, and a nitrogen bridge is established, forming extended chains of cooperative hydrogen bonds [15]. Monitoring the action of LPMOs on modified cellulose structures may give more insight into LPMO specificity to identify the key structural cellulose patterns that favor the LPMO action.

A recent study investigated the action of LPMOs on native cellulose I, cellulose II and amorphous cellulose, revealing a great functional variation among the cellulose-active LPMOs tested, with an important influence of the appended carbohydrate binding module (CBM) [16]. In this work, we present a complementary study focused on the molar mass decrease and the peeling effect of LPMOs on different allomorphs of cellulose: cellulose I, II, III and amorphous cellulose. We investigated the action of two LPMO enzymes from *Podospora anserina: Pa*LPMO9E and *Pa*LPMO9H, both containing a CBM1 module. *Pa*LPMO9E preferentially cleaves cellulose at the C1 position, and *Pa*LPMO9H mainly attacks at the C4 position together with some C1 oxidation. Using molar mass monitoring, we revealed the different activity of *Pa*LPMO9E and *Pa*LPMO9H enzymes on the three cellulose allomorphs.

2. Materials and Methods

2.1. Materials

Cysteine, copper sulfate, sodium acetate, acetic acid, sodium hydroxide, ethylenediamine (EDA), lithium chloride (LiCl), and monochloroacetic acid (MCA) were purchased from Sigma-Aldrich. *N*,*N*-dimethylacetamide (DMAc) and methanol were purchased from ThermoFisher Scientific. Isopropanol was supplied by VWR International. The recombinant *Pa*LPMO9E and *Pa*LPMO9H enzymes from *Podospora anserina* [17] were produced in *Pichia pastoris* in a 1 L bioreactor and purified as previously described [18]. The molar masses of *Pa*LPMO9E and *Pa*LPMO9H were 31.36 kDa and 33.21 kDa, respectively. Cellulose from cotton linters (cellulose I) was used as the cellulose substrate. Whatman paper was hydrated in water under stirring for 24 h and activated in a blender at 25 g L^{-1}, and finally pulp was freeze-dried.

2.2. Cellulose allomorph preparation

Cellulose II fibers (Cell-II) were prepared from cellulose I (Cell-I) pulp, as previously described [19]. 2 g of pulp was soaked in a freshly prepared solution of NaOH 20% at a final volume of 60 mL. The dispersion was magnetically stirred at room temperature for 5 h. It was then filtered with a polycarbonate membrane (5 µm) and washed with ultrapure water until the filtrate was neutral. The obtained fibers were freeze-dried.

Cellulose III fibers (Cell-III) were prepared from cellulose I pulp, as previously described [20] by soaking 0.9 g of pulp in ethylenediamine (EDA) at 75% at a final volume of 30 mL. The dispersion was stirred on a rotating mixer at 27 °C for 1 h, and the excess of EDA was removed by filtration. The pulp was then washed with methanol until the filtrate was neutral and filtered with a polyvinylidene fluoride (PVDF) membrane (47 µm). The fibers were left to dry overnight under the hood before being freeze-dried.

Phosphoric acid swollen cellulose (PASC) was prepared from cellulose I pulp, as previously described [21]. 1 g of pulp was soaked in 20 mL of a solution of phosphoric acid at 85% at 4 °C overnight. 80 mL of ultrapure water was added and the mixture was stirred magnetically and with a spatula until homogeneity. It was then filtered with a polycarbonate membrane (5 µm) and washed with water (2 x 250 mL), sodium bicarbonate at 1 % (3 x 250 mL) to neutralize the acid and again with water until neutral pH (2 x 250 mL). The PASC was then freeze-dried for storage.

2.3. LPMO treatment

LPMO treatment of cellulose fibers was performed at the conditions previously determined for optimal LPMO activity [12]. Briefly, cellulose fibers (100 mg) were dispersed in acetate buffer (50 mM) adjusted at the desired pH (5.2) at a final reaction volume of 20 mL. Purified *Pa*LPMO9E or *Pa*LPMO9H enzyme was added to the pulps at a final concentration of 16 mg g^{-1} (2.6 and 2.4 µM, respectively) and cysteine at 48 mg g^{-1} (50 mM). Enzymatic incubation was performed at 26.6 ºC under mild agitation for 48 h. LPMO enzyme was deactivated by heating at 100 ºC for 10 min. The reference samples were subjected to the same treatment but they contained copper sulfate (48 nmol) instead of the enzyme. The fibers were then filtered on a polycarbonate (PC) membrane of 5 µm, rinsed with water and freeze-dried for further analyses.

2.4. Carboxymethylation

Carboxymethylated cellulose was prepared as previously described [22]. Enzyme-treated cellulose fibers (~100 mg) were rinsed with isopropanol and filtered on a polycarbonate (PC) membrane (5 µm). Monochloroacetic acid (10 mg) was solubilized in isopropanol at a final volume of 0.5 mL. The fibers were soaked in this solution for 30 min. In a round-bottom flask, sodium hydroxide (16 mg) was solubilized in isopropanol (1 mL) at 60 °C under stirring until complete solubilization. The fibers were added in the flask and stirred at 70 °C

for 1 hour. They were filtered on a PC membrane (5 µm) and rinsed three times with isopropanol and three times with water until neutral pH. The fibers were freeze-dried before further analyses.

2.5. Monosaccharide analysis

Identification and quantification of cellulose allomorphs neutral monosaccharide composition before and after LPMO action were performed by gas-liquid chromatography (GC) after sulfuric acid degradation [23]. Pulps were ground under cryogenic conditions into a fine powder using the SPEX 6700 Freezer Mill, and dried at 40 °C in a vacuum oven containing P_2O_5 for 48 h. A previse mass of about 5 mg of dried pulps were dispersed in 12 M sulfuric acid for 1h at 30 °C and then hydrolyzed in 1 M sulfuric acid (2 h, 100 °C). Monosaccharides released were converted to alditol acetates according to Quemener et al. [24] and analyzed by a TRACE™ Ultra Gas Chromatograph (Thermo Scientific™; temperature 205 °C, carrier gas H_2). Standard monosaccharide solution (Sigma) and inositol as internal standard were used for calibration. Experiments were done in triplicate.

2.6. Polarized optical microscopy

Cellulose fibers (0.1 g L^{-1}) were fixated onto a glass slide and dried at 40°C. Morphology was observed by a BX51 polarizing microscope (Olympus France S.A.S.) using a 4× objective. Images were recorded by a U-CMAD3 camera displaying a U-TV0.5XC-3 adaptor (Olympus Japan). At least 20 images were recorded from each sample to assure representative results.

2.7. Scanning electron microscopy (SEM)

Cellulose fibers (0.1 g L^{-1}) were applied onto an adhesive carbon pad and dried at room temperature. Images were obtained by a Quattro scanning electron microscope at low-vacuum (Thermo Scientific).

2.8. Infrared analysis (FT-IR)

Cellulose fibers (2 mg) were freeze-dried and mixed with KBr to prepare pellets. Infrared spectra were recorded by a Nicolet iS50 FTIR spectrometer (Thermo Scientific) in the absorbance mode. All spectra were collected with a 4 cm^{-1} resolution after 200 continuous scans from 400 to 4000 cm^{-1}.

2.9. X-Ray diffraction

Cellulose samples (10 mg) were freeze-dried and pressed in a hydraulic press (10 T) to prepare circular discs with a 1 cm diameter. The X-ray diffractograms were recorded by a Bruker D8 Discover diffractometer with a Ni-filtered Cu $K_{\alpha 1}$ radiation (Cu $K_{\alpha 1}$ = 1.5405 Å), produced in a sealed tube at 40 kV and 40 mA, which was selected and parallelized using a Gobël parallel optics mirror system, and then collimated to produce a 500 µm beam diameter. X-ray diffraction data were collected using a Bruker Vantec500 two-dimensional detector. Crystallinity was calculated from the XRD patterns of cellulose according to the Segal method [25].

2.10. High Performance Size Exclusion Chromatography (HPSEC)

Molar mass of cellulose chains was determined as previously described [5]. Briefly, fibers (80 mg) were firstly filtered over sinter glass (porosity 16-40 µm) to remove water, and then dispersed in anhydrous methanol (3×20 mL). After methanol removal by filtration, fibers were dispersed in anhydrous dimethylacetamide (DMAc) (3×20 mL). Then the DMAc-swollen fibers were added to 8 mL of DMAc/LiCl (9% *w*/*w*) under magnetic stirring during 1 to 3 days at 4 °C, and finally 10-fold diluted with anhydrous DMAc. The dispersion was then filtered (PTFE 0.45 µm) and injected on a size exclusion chromatography system (OMNISEC Resolve, Malvern) using DMAc/LiCl (0.9% *w/v*) as the eluent. For Cell-I, Cell-II and Cell-III, the analysis was conducted in triplicate to calculate the mean results while the analysis for PASC was conducted in duplicate. The SEC columns used were Viscoteck Tguard, LT4000L, LT5000L and LT7000L. The system was equipped with a multi-angle laser light scattering

Malvern SEC-MALS 20 and OMNISEC Reveal devices (Malvern). Calculations were performed with a *dn/dc* value of 0.136 mL g^{-1} and performed using OMNISEC software.

2.11. Conductometry

The carboxylate content of the cellulose fibers was measured by conductometric titration. Dry fibers (80 – 100 mg) were dispersed in MilliQ water (10 mL). The dispersion was divided in duplicates of 5 mL and hydrochloric acid (0.01 M) was added to a final volume of 10 mL. The solution was titrated by a solution of sodium hydroxide (0.01 M) by a 800 Dosino dosing device coupled with a 807 Dosing Unit, a 856 Conductivity Module and a 801 Stirrer. The titration set-up was controlled by the software *Tiamo*™ from Metrohm. The carboxylate content of the fibers was calculated as follows:

$$Carboxylate\ content\ \left(\frac{mmol}{g}\right) = \frac{C_{NaOH}V_{NaOH}}{m_{fibers}} = \frac{n_{COOH}}{m_{fibers}}$$

Where C_{NaOH} is the concentration of sodium hydroxide (0.01 M), V_{NaOH} is the volume of sodium hydroxide needed to neutralize all the COOH groups, n_{COOH} is the number of equivalents of COOH groups, calculated from conductometric titration, and m_{fibers} is the dry mass of the titrated pulp.

For Cell-I, Cell-II and Cell-III, 3 to 5 repetitions were done to calculate the average charge density, and 2 repetitions were carried out for PASC.

3. Results

3.1. Preparation and characterization of cellulose allomorphs

Native cotton linters (Cell-I) were submitted to NaOH and EDA treatments to obtain the crystalline allomorphs cellulose II (Cell-II) and cellulose III (Cell-III), respectively; and to H_3PO_4 to prepare amorphous cellulose (PASC). **Fig. 1** shows the scheme of the cellulose transformation, and the polarized optical microscopy images of the three crystalline cellulose allomorphs and amorphous cellulose.

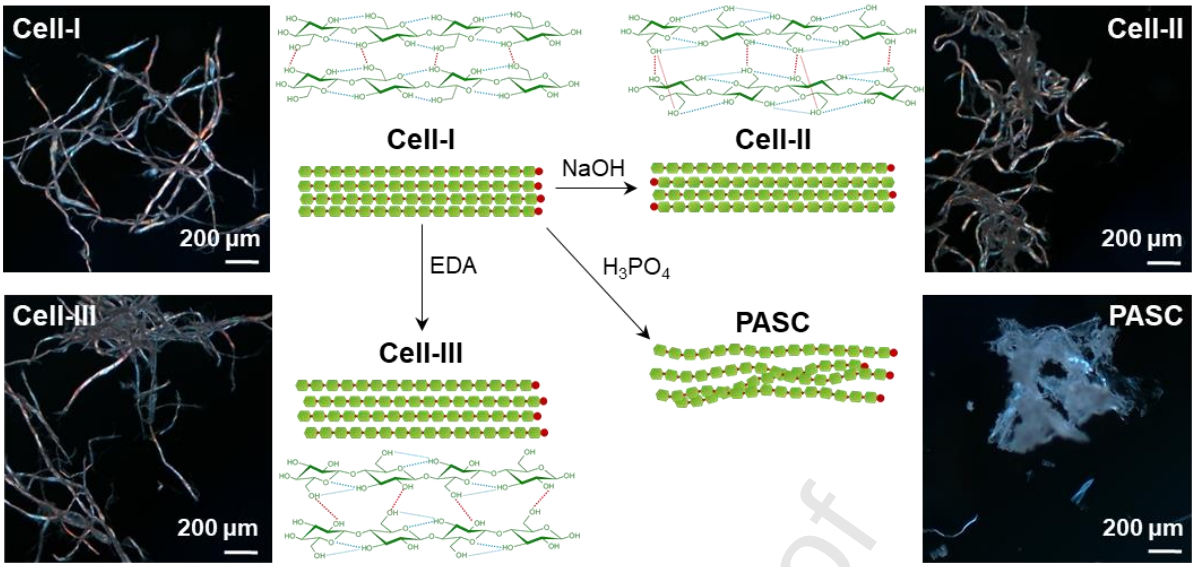

Fig. 1. Pathways for cellulose I conversion and representative polarized optical microscopy images of native cellulose fibers (Cell-I), NaOH-treated (Cell-II), EDA-treated (Cell-III), and phosphoric acid swollen cellulose (PASC).

Based on microscopy images, the fiber dimensions and morphology seemed to be similar for all allomorphs; however, the treatment with NaOH or EDA resulted in higher aggregation of the cellulose fibers. Both Cell-II and Cell-III seemed more swollen and agglomerated than Cell-I, forming a tight network of fibers with inter-ribbon interactions. Cell-II seemed more tortuous and sometimes twisted, which could be attributed to swelling in NaOH and the subsequent shrinkage and collapse during the purification steps [26]. PASC showed highly disrupted fiber forming an interconnected and continuous network.

FT-IR was used to distinguish between the different cellulose allomorphs (**Fig. 2**). The spectrum of Cell-I showed the characteristic bands for this allomorph [14, 27]: the hydrogen-bonded OH stretching at ca. 4000-2995 cm^{-1}, the CH stretching at 2900 cm^{-1}, the HCH and OCH bending vibrations at 1430 cm^{-1}. By the transformation of Cell-I to Cell-II, several characteristic bands were shifted at the peak maximum (**Fig. 2**c). For the PASC, a shift from

3348 to 3400 cm^{-1} was observed as the main difference from Cell-I. The main band shifts are summarized in **Fig. 2**c.

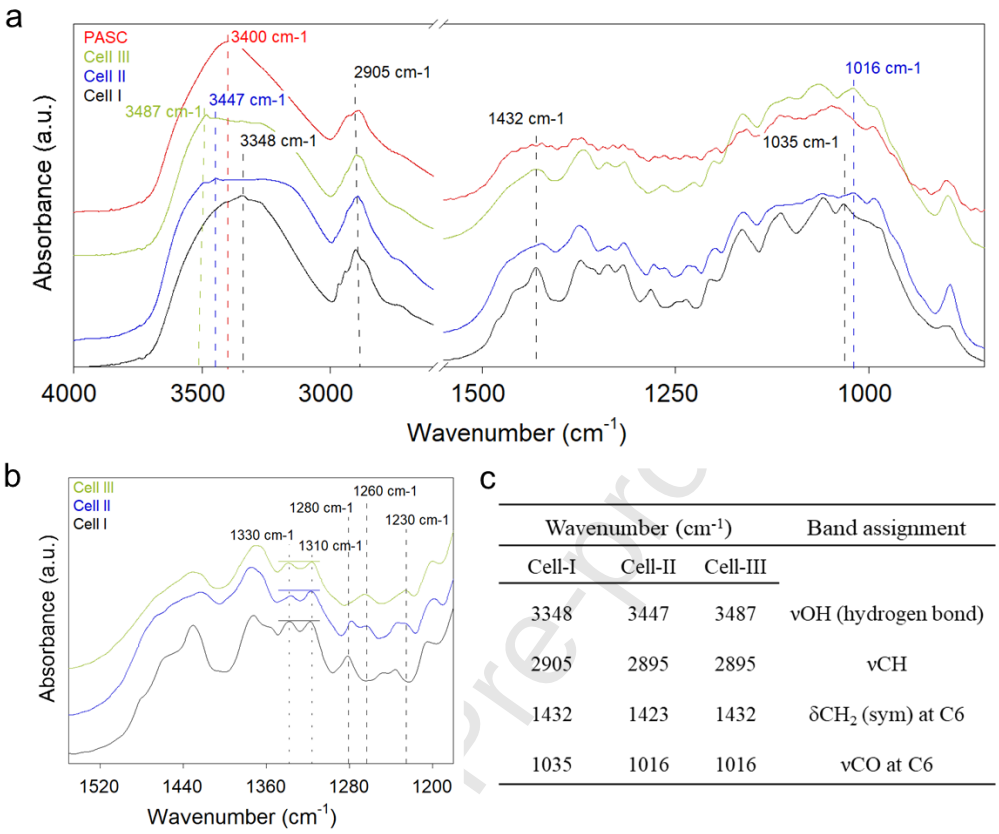

c

Wavenumber (cm^{-1})			Band assignment
Cell-I	Cell-II	Cell-III	
3348	3447	3487	νOH (hydrogen bond)
2905	2895	2895	νCH
1432	1423	1432	δCH_2 (sym) at C6
1035	1016	1016	νCO at C6

Fig. 2. FT-IR spectra of native cellulose fibers (Cell-I), NaOH-treated (Cell-II), EDA-treated (Cell-III), and phosphoric acid-treated (PASC): full spectra (a), and focus on the 1500-1100 cm^{-1} region (b). Main FT-IR bands related to the transformation of Cell-I into Cell-II or Cell-III, and their assignments according to the literature (c).[14]

The changes in FT-IR were less visible between Cell-I and Cell-III, but a shift from 3348 to 3487 cm^{-1} was observed at the OH stretching region. In all allomorphs, there are some characteristic bands, shown in **Fig. 2**b, which have the same wavenumber but show different peak intensity, which allows differentiating between the three allomorphs: the two bands at 1310 and 1330 cm^{-1}, ascribed to OH stretching and bending [28], respectively, and the group of three bands at 1230, 1260 and 1280 cm^{-1} [29], assigned to C6-OH, C2,3-OH, and C-H

bendings [14], respectively. For Cell-I, the bands at 1310 and 1330 cm^{-1} were equally in absorbance whereas for Cell-II and Cell-III, the band at 1310 cm^{-1} was stronger in intensity. Concerning the bands at 1230, 1260 and 1280 cm^{-1}, the changes were very small: Cell-I presented a stronger band at 1280 cm^{-1}, followed by the bands at 1230 and 1260 cm^{-1}; Cell-II and Cell-III presented a stronger band at 1230 cm^{-1}, followed by the bands 1280/1260 and 1260/1280 respectively.

X-ray diffraction (XRD) patterns of all allomorphs are shown on **Fig. 3**. For Cell-I, the diffraction peaks at 2θ at 14.5°, 16.5° and 22.5° were attributed to the planes $(1\bar{1}0)$, (110) and (200) respectively, which corresponds to the characteristic diffraction peaks of cellulose I [30, 31]. For Cell-II, the diffraction peaks at 2θ were observed at 12.0° for the plane $(1\bar{1}0)$, at 20.0° for the plane (110) and at 22.0° for the plane (020) [30, 31]. For Cell-III, the characteristic diffraction peaks at 2θ at 11.7°, 17.3° and 21.0° were attributed to the (010), (002) planes and a composite of (100), (012) and $(1\bar{1}0)$ planes, respectively. Weak peaks (2θ around 14.5° and 16.5°) of cellulose I were also detected but they were less obvious [30]. The XRD pattern of PASC showed the characteristic pattern of amorphous cellulose. All these observations showed that the conversions from Cell-I to the various allomorphs were successfully achieved.

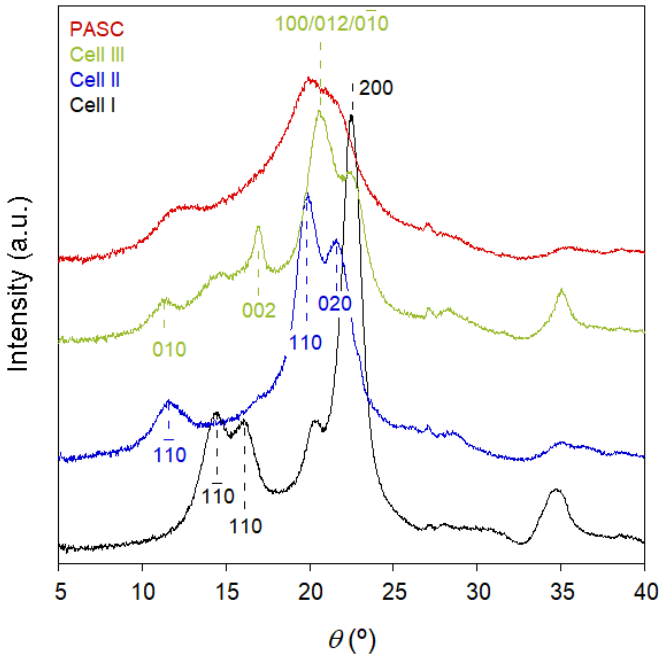

Fig. 3. XRD patterns of native cellulose fibers (Cell-I), NaOH-treated (Cell-II), EDA-treated (Cell-III), and phosphoric acid-treated (PASC).

Crystallinity, calculated from the XRD spectra, were 60%, 43% and 50% pour Cell-I, Cell-II and Cell-III, respectively.

3.2. LPMO effect on the different cellulose allomorphs

The different cellulose allomorphs were treated with two different LPMO enzymes (*Pa*LPMO9E and *Pa*LPMO9H), displaying different regioselectivities (C1 and mainly C4, respectively). Scanning electron microscopy (SEM) images was used to visualize the impact of the enzymes on fiber morphology (Fig. **4**).

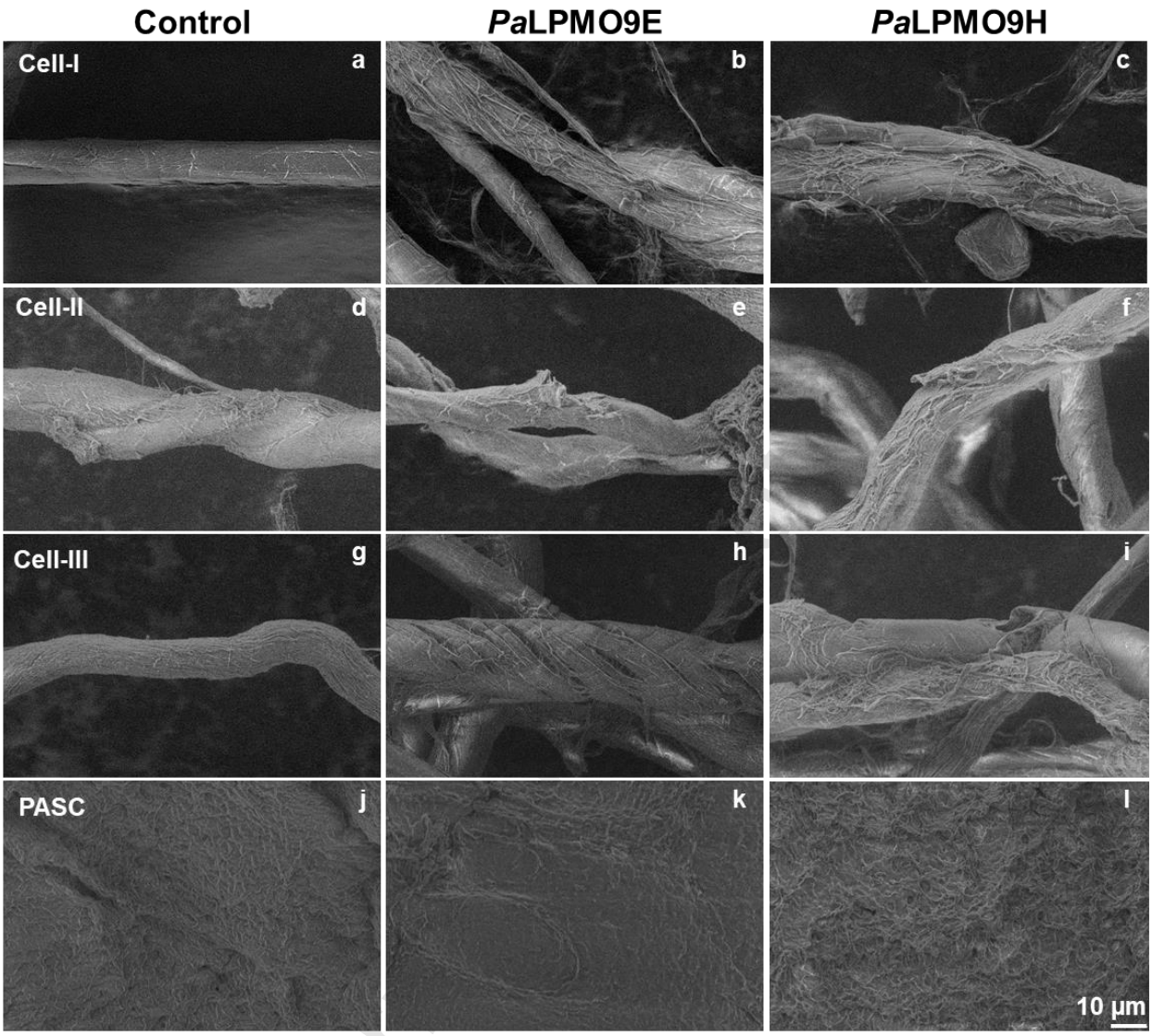

Fig. 4. Morphology of LPMO-treated celluloses: Scanning electronic microscopy (SEM) images of native cellulose fibers (Cell-I) (a-c), NaOH-treated (Cell-II) (d-f), EDA-treated (Cell-III) (g-i), and phosphoric acid-treated (PASC) (j-l) for control fibers (a, d, g, j) and after *Pa*LPMO9E (b, e, h, k) or *Pa*LPMO9H (c, f, i, l) treatments with enzyme concentration of 16 mg g^{-1} and cysteine concentration of 48 mg g^{-1}, at pH 5.2 and 26.6 ºC for 48 h.

Control Cell-I, Cell-II and Cell-III fibers showed a rather smooth surface. They appeared to be ribbon-like and occasionally fibers turn along the long axis, presenting some twists (Fig. **4**a, d and g) whereas PASC showed totally disrupted fibers forming a uniform surface (Fig. **4**j). Upon incubation with *Pa*LPMO9E or *Pa*LPMO9H, surface roughness increased as

enzymes seemed to create a characteristic pattern of cracks and wrinkles in the outer layer of the fiber surface that disrupted the fiber structure (Fig. **4**b, e and h for *Pa*LPMO9E, and c, f and i for *Pa*LPMO9H). This enzymatic action has been previously observed for cellulose I treated with *Pa*LPMO9H, and was ascribed to the LPMO attack at the tension regions of the fiber [12]. Thus, LPMO enzymes seemed to peel the cellulose surface, which may increase the accessibility and swelling. By SEM images, no significant differences were observed between the action of *Pa*LPMO9E or *Pa*LPMO9H on the three cellulose allomorphs (Cell-I, Cell-II and Cell-III). In the case of PASC, no noticeable change was observed upon enzymatic action.

The LPMO activity was monitored as the changes in the molar mass distribution. For this purpose, the cellulose fibers were solubilized in DMAc/LiCl and analyzed by high performance size exclusion chromatography (HPSEC). HPSEC data allowed the calculation of average weight molar mass (M_w), the average number molar mass (M_n), the degree of polymerization (*DP*), and the polydispersity index (M_w/M_n) for the different cellulose allomorphs treated with both LPMO enzymes (Table 1 and Table S1).

Table 1

Weight average molar mass (M_w), number average molar mass (M_n), and polydispersity (M_w/M_n) of native cellulose fibers (Cell-I), NaOH-treated (Cell-II), EDA-treated (Cell-III), and phosphoric acid-treated (PASC) for control fibers and after *Pa*LPMO9E or *Pa*LPMO9H treatment with enzyme concentration of 16 mg g^{-1} and cysteine concentration of 48 mg g^{-1}, at pH 5.2 and 26.6 ºC for 48 h.. Results are expressed as mean ± standard deviation.

M_w (10^3 g mol^{-1})	Cell-I	Cell-II	Cell-III	PASC
Control	400 ± 28	334 ± 16	400 ± 24	166 ± 58
*Pa*LPMO9E	371 ± 43	321 ± 13	380 ± 36	135 ± 34
*Pa*LPMO9H	326 ± 43	313 ± 5	369 ± 37	122 ± 14

M_n (10^3 g mol^{-1})	Cell-I	Cell-II	Cell-III	PASC
Control	207 ± 18	159 ± 47	227 ± 4	75 ± 25
*Pa*LPMO9E	215 ± 25	176 ± 18	219 ± 24	80 ± 41
*Pa*LPMO9H	166 ± 49	125 ± 19	177 ± 43	65 ± 7
M_w/M_n	Cell-I	Cell-II	Cell-III	PASC
Control	1.95 ± 0.32	2.24 ± 0.65	1.77 ± 0.08	2.21 ± 0.04
*Pa*LPMO9E	1.73 ± 0.14	1.83 ± 0.12	1.74 ± 0.03	1.83 ± 0.52
*Pa*LPMO9H	2.03 ± 0.31	2.54 ± 0.42	2.16 ± 0.50	1.87 ± 0.03

A satisfactory recovery yield (Table S1) was obtained for all cellulose allomorphs (> 79%), indicating good dissolution of the cellulose fibers and a suitable set-up to avoid sample loss during sample preparation and analysis. After LPMO incubation, the recovery was even higher, suggesting that no or very little soluble sugars were released, as previously observed for *Pa*LPMO9H [4, 12].

Concerning the molar masses before LPMO treatment, control samples presented lower average values for Cell-II and PASC than native Cell-I. In the case of Cell-II, the decrease might be ascribed to partial cellulose hydrolysis by NaOH; and for PASC, the lower molar mass could be due to acid hydrolysis of cellulose chains, which significantly reduces the molar mass and the polydispersity index. Upon incubation with *Pa*LPMO9E or *Pa*LPMO9H, the average molar mass (M_w) of all allomorphs decreased, showing more pronounced decrease when incubated with *Pa*LPMO9H than with *Pa*LPMO9E (**Fig. 5** e). The molar mass distributions for each cellulose reflected this behavior by the appearance of a new low molar mass fraction after the LPMO action (**Fig. 5** a-d).

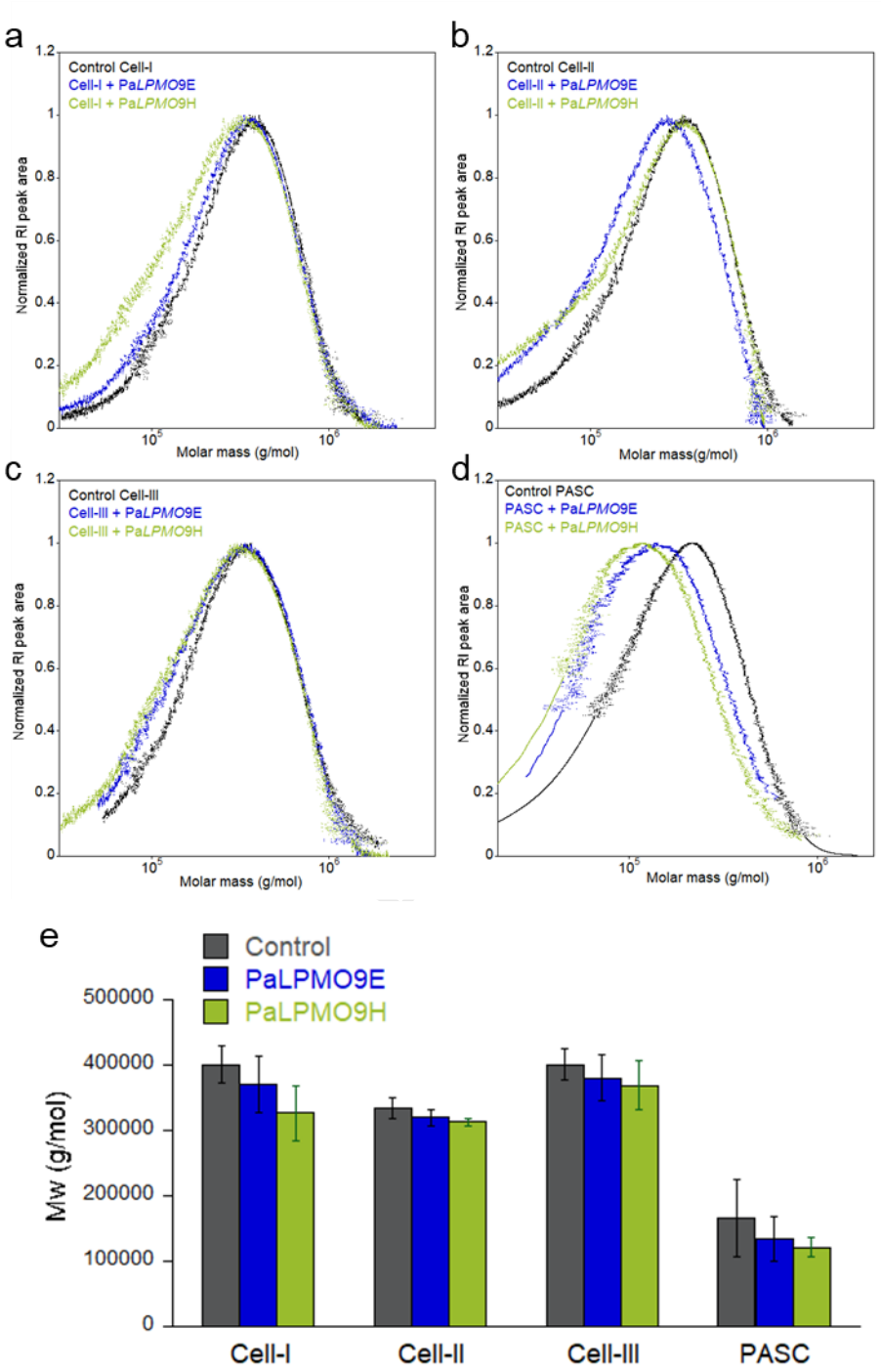

Fig. 5. Molar mass distribution profiles of native cellulose fibers (Cell-I) (a), NaOH-treated (Cell-II) (b), EDA-treated (Cell-III) (c), and phosphoric acid-treated (PASC) (d) for control fibers and after *Pa*LPMO9E or *Pa*LPMO9H treatment with enzyme concentration of 16 mg g^{-1} and cysteine concentration of 48 mg g^{-1}, at pH 5.2 and 26.6 ºC for 48 h. Weight average molar mass (M_w) values (e).

Comparing the different types of cellulose, the higher molar mass decrease was observed for PASC samples treated with *Pa*LPMO9E or *Pa*LPMO9H, and Cell-I treated with *Pa*LPMO9H. The decrease for both weight average molar mass (M_w) and number average molar mass (M_n) showed the same tendency PASC > Cell-I > Cell-III > Cell-II, for both enzymes. Stopamo et al. showed how different LPMOs bound to PASC to an higher extent and to Cell-II to a lower extent than to Cell-I [16]. Both *Pa*LPMO9E and *Pa*LPMO9H hold a CBM1; therefore, the molar mass decrease could be correlated to the LPMO binding on the cellulose surface. This is in agreement with the higher accessibility of PASC, and better affinity of LPMOs to Cell-I compared to the other allomorphs.

From the degree of polymerization (DP_n) calculated from M_n, the chain scission (S) can be determined according to the following expression [32]:

$$S = \frac{1}{DP_n^{end}} - \frac{1}{DP_n^0}$$

Where $DP_n^{\,0}$ and $DP_n^{\,end}$ are the degrees of polymerizations at time zero and at the end of the LPMO incubation, respectively. Table 2 reviews the values of S for the different celluloses treated with both LPMO enzymes.

Table 2

Number of chain scissions, S (μmol 100 g^{-1}), for native cellulose fibers (Cell-I), NaOH-treated (Cell-II), EDA-treated (Cell-III), and phosphoric acid-treated (PASC) after *Pa*LPMO9E (C1 oxidation) or *Pa*LPMO9H (mostly C4 oxidation) treatment with enzyme concentration of 16 mg g^{-1} and cysteine concentration of 48 mg g^{-1}, at pH 5.2 and 26.6 ºC for 48 h.

S (mmol $100g^{-1}$)	Cell-I	Cell-II	Cell-III	PASC
*Pa*LPMO9E	< 0	< 0	0.016	< 0
*Pa*LPMO9H	0.119	0.171	0.124	0.205

The number of chain scissions would reveal clear differences between the modes of action of both enzymes on the different types of cellulose. For *Pa*LPMO9E, the number of chain scissions was very low or negative, suggesting that very few new chains were formed upon *Pa*LPMO9E action. Concomitantly, M_w decreased, which could suggest that *Pa*LPMO9E attacks at the chain ends, with the release of soluble oligomers that decrease M_w but they are not quantified by HPSEC. This hypothesis was reinforced by the decrease of the polydispersity index after *Pa*LPMO9E incubation, which pointed at narrower distributions for all celluloses upon the *Pa*LPMO9E action (**Fig. 5**).

Differently, *Pa*LPMO9H showed chain scission between 0.1 and 0.2 mmol 100 g^{-1} for all allomorphs, in agreement with the values obtained by Sulaeva et al. [32]. The number of chain scissions decreased according to the following tendency: PASC > Cell-II > Cell-III > Cell-I. Apart from PASC, which was highly attacked by LPMOs, the number of chain scissions showed the opposite behavior than the M_w decrease. Thus, Cell-I, which presented a decrease in M_w of 20% after *Pa*LPMO9H action, showed the lower chain scission (0.119 mmol 100 g^{-1}) than Cell-II, whose M_w decrease was 4% but presented higher chain scission (0.171 mmol 100 g^{-1}). The higher decrease in M_w could therefore be ascribed to more efficient enzyme binding to the Cell-I surface, as Stopamo et al. proposed [16]. When cellulose was treated with NaOH or EDA, the disruption of the native hydrogen bonding network might increase the accessibility of the cellulose chains; nevertheless, the less efficient enzyme binding could result in LPMO action on the surface cellulose chains while leaving the underlying chains less affected and largely intact. The higher chain scission observed for *Pa*LPMO9H-treated cellulose allomorphs was confirmed by the increase of the polydispersity index, suggesting the formation of broader molar distributions, with a new small molar mass fraction, especially for Cell-I and Cell-II (**Fig. 5**).

Regarding the non-cellulosic monosaccharide profile, both Cell-II and PASC did not show any significant change after LPMO treatment. For Cell-I and Cell-III, the amount of xylose and rhamnose decreased after *Pa*LPMO9E or *Pa*LPMO9H treatment, which could suggest the release and/or hydrolysis of hemicelluloses (Table S2).

In order to demonstrate the increase in accessibility after the LPMO treatment, we performed carboxymethylation reactions on the different cellulose allomorphs pretreated with *Pa*LPMO9E or *Pa*LPMO9H enzymes. Carboxymethylation is a Williamson's etherification that grafts carboxymethyl groups on the C2, C3 and C6 hydroxyl groups from cellulose. Cellulose fibers were firstly impregnated with monochloroacetic acid, and then the hydroxyl groups were activated by NaOH to avoid complete dissolution of cellulose chains. Fig. **6** shows the carboxylate content after carboxymethylation for control and LPMO-pretreated celluloses.

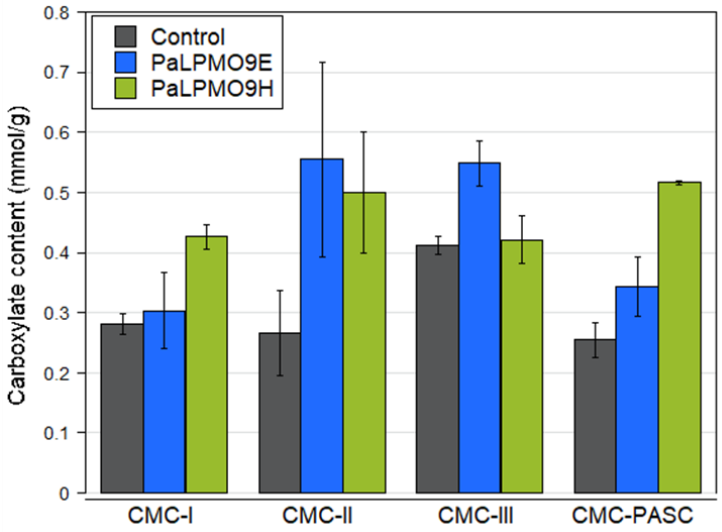

Fig. 6. Carboxylate content of carboxymethylated native cellulose fibers (CMC-I), NaOH-treated (CMC-II), EDA-treated (CMC-III) and phosphoric acid-treated (CMC-PASC) for control samples and samples pretreated with *Pa*LPMO9E or *Pa*LPMO9H with enzyme concentration of 16 mg g^{-1} and cysteine concentration of 48 mg g^{-1}, at pH 5.2 and 26.6 ºC for 48 h.

Before carboxymethylation, for all allomorphs except for PASC, the average charge density of the controls was around 0.05-0.1 mmol g^{-1} (Fig. S1). The presence of carboxylic acid groups in cellulose fibers could be due to partial oxidations during the pulp pretreatments [33]. Upon incubation with LPMO enzymes, a slight increase of charge density was observed before carboxymethylation for all crystalline cellulose allomorphs. Differently, the surface charge increased significantly when PASC was incubated with *Pa*LPMO9E or *Pa*LPMO9H (Fig. S1). The increase of carboxylate content upon LPMO action has already been observed for cellulose fibers [34, 35], microcrystalline cellulose [36] and cellulose nanocrystals [37, 38]. On cellulose fibers, increase of surface charge is 0.050-0.065 mmol g^{-1} [35] but can reach up to 0.70 mmol g^{-1} with a *Nc*LPMO9F that does not display a CBM1 [36]. In our study, both *Pa*LPMO9E and *Pa*LPMO9H hold a CBM1, but differ in terms of regioselectivity. Therefore, fibers treated with *Pa*LPMO9E should present higher surface charge, as the enzyme generates carboxylic acids at the C1 position, while *Pa*LPMO9H action mainly lead to aldehyde groups at the C4 position.

In a second step, we investigated the increase in accessibility to chemicals resulting from the LPMO action on the fibers. When samples were carboxymethylated, the different types of cellulose pretreated with LPMO enzymes showed an increase in the carboxymethyl content, compared to the carboxymethylated control samples without LPMO treatment (**Fig. 6**). This effect was less evident for Cell-I treated with *Pa*LPMO9E and Cell-III pretreated with *Pa*LPMO9H. Overall, carboxymethylation reaction demonstrated an increase in the surface accessibility to chemicals (monochloroacetic acid) upon LPMO action. As previously described [4, 12], LPMOs seem to create nicking points that may increase the accessibility to water [39], chemicals or other enzymes. Breaking the glycosidic bond and introducing

oxidized groups may cause steric effects that improve the accessibility of the hydroxyl groups of cellulose, allowing a higher efficiency of the carboxymethylation reaction.

4. Discussion

In this study, we have shown using different methodologies that both *Pa*LPMO9E and *Pa*LPMO9H enzymes are active on the different cellulose allomorphs, Cell-I, Cell-II and Cell-III, and on amorphous cellulose (PASC). In more details, both enzymes behaved differently on the diverse types of cellulose. *Pa*LPMO9H seemed to be more active than *Pa*LPMO9E, and this effect was more pronounced on the cellulose I allomorph. Song et al. postulated that TrAA9A exhibited random movement along, across, and penetrating into the ribbon-like structure of cellulose [40]. Thus, *Pa*LPMO9H could exhibit all movements, especially across and/or penetrating the cellulose surface by cutting chains and releasing long chains that increase polydispersity. Differently, *Pa*LPMO9E seemed to exhibit along movement, attacking at the chain ends and decreasing molar mass without generating high molar mass chain fragments. This behavior results in narrower molar mass distributions and lower polydispersity indexes.

As previously shown, the highest activity of both enzymes was observed on PASC. The swelling and disruption of the cellulose fiber by phosphoric acid results in a highly accessible surface, where LPMOs can easily bind and oxidatively cleave the chains [16]. The action on the different cellulose allomorphs demonstrated that LPMOs have a specificity on the cellulose native crystalline structure; as we observed that the activity was higher in the allomorph whose hydrogen bonding pattern had not been altered (Cell-I). Indeed, the decrease in M_w was correlated with the crystallinity calculated by XRD. Thus, the higher the crystallinity (60% for Cell-I versus 43% for Cell-II), the higher the M_w reduction (20% and 4% for Cell-I and Cell-II, respectively). Mudedla et al. postulated that the chain peeling

involves first the breaking of hydrogen bonds formed by the O2H and O6' groups, followed by the formation of new hydrogen bonds by the O3H3 groups [41]. *Pa*LPMO9E and *Pa*LPMO9H could therefore show higher specificity to Cell-I bonding pattern, which is in agreement with more efficient enzyme binding to cellulose I compared to other allomorphs, as previously described [16]. The higher activity on the cellulose I allomorph contrasts with the opposite effect observed for cellulases. Hence, different studies have demonstrated that the cellulases' hydrolytic action increased in the sequence Cell-I < Cell-III < Cell-II [42-45], which was correlated to the higher accessibility to enzymes [46]. This behavior could explain the synergy between cellulases and LPMOs in cellulose degradation [40, 47], so LPMOs could attack more recalcitrant cellulose I structures and increase their accessibility for cellulases. For Cell-I, *Pa*LPMO9H may start breaking surface chains and continue digging into the fiber, so that the Cell-I arrangement is more favorable for *Pa*LPMO9H attack than the separated chains in Cell-III or the antiparallel in Cell-II. Therefore, across and/or penetrating action of LPMOs seems to be inhibited when the cellulose I structure is disrupted. This hypothesis was confirmed by the decrease in M_w (and the polydispersity increase), and the cracks observed by SEM (**Fig. 4**), and supports the theory of disruption of tension regions where cellulose chains are tightly packed (twists) [12]. Therefore, the formation of a new crystalline structure in Cell-III, even if the accessibility increases, does not boost the LPMO activity. Indeed, the antiparallel arrangement of cellulose chains in Cell-II is not favorable for LPMO action. The same behavior has been recently described by Stopamo et al., who ascribed it to lower enzyme binding to cellulose II [16]. Our work corroborates that LPMOs are active on both disordered and crystalline cellulose, and demonstrates some specificities linked to the crystalline structure. Hence, the studied LPMOs presented more activity on the cellulose I allomorph, even if it is the most crystalline structure. It might indicate a specificity of LPMOs for the native hydrogen pattern, which could be associated not only to the enzyme

binding but also to the LPMO mechanism of action. For *Pa*LPMO9H, which released high molar mass fragments, this effect was more pronounced than for *Pa*LPMO9E, which appeared to act at chain ends. Therefore, LPMOs seem to have some preference for the cellulose I crystalline lattice, whose degradation could be the starting point for the enzymatic deconstruction of cellulose by other enzymes, like cellulases.

5. Conclusions

This work describes the action of two different LPMOs from *Podospora anserina*, *Pa*LPMO9E and *Pa*LPMO9H, on celluloses showing different structural patterns: three cellulose allomorphs (I, II and III), and amorphous cellulose (PASC). Both LPMOs were active on the different cellulose allomorphs (I, II and III), and on PASC whereas they displayed a different behavior, with a higher molar mass decrease observed for cellulose I. *Pa*LPMO9H seemed to be more active than *Pa*LPMO9E, and this effect was more pronounced on cellulose I. *Pa*LPMO9H seemed to act on the cellulose surface by cutting chains and releasing long chains; whereas *Pa*LPMO9E appeared to cleave at the chain end, which decreased molar mass but did not generate new fragments. Overall, the pretreatment with LPMO enzymes increased accessibility of all types of cellulose, which was quantified by the higher carboxylate content after carboxymethylation reaction on LPMO-pretreated celluloses. This work gives understanding of the action of enzymes to obtain new cellulose-based materials for different applications. Even if LPMOs are promising tools for biomass deconstruction, there are still limitations associated to the quantification of enzymatic action, and the specificity of each enzyme towards each type of cellulosic substrate. Therefore, as demonstrated in this study, the combination of different techniques is required to evaluate and characterize LPMO action on the insoluble part of the cellulose fiber.

CRediT authorship contribution statement

M.G.: Conceptualization, Investigation, Visualization, Writing—original draft, Writing—review & editing.

C.M.: Conceptualization, Investigation, Writing—review & editing.

J.B.: Investigation, Writing—review & editing.

S.G.: Investigation, Writing—review & editing.

J.G.B.: Conceptualization, Investigation, Project administration, Funding acquisition, Writing—review & editing.

B.C.: Conceptualization, Investigation, Project administration, Writing—review & editing.

A.V.: Conceptualization, Investigation, Project administration, Supervision, Visualization, Writing—original draft.

All authors have read and agreed to the published version of the manuscript.

Declaration of competing interest

The authors declare that they have no known competing financial interests or personal relationships that could have appeared to influence the work reported in this paper.

Data availability

The datasets generated during the current study are available from the corresponding author on reasonable request.

Acknowledgements

The authors gratefully acknowledge the 3BCar Carnot Institute for financial support (Fonzy project). The authors acknowledge Lèna Brionne for the monosaccharide analysis, and the BIBS platform of INRAE for the access to electronic microscopy (Bruno Novales) and X-ray

(Hyazann Hulin) facilities. Part of the work described was performed using services provided by the 3PE platform, a member of IBISBA-FR (https://doi.org/10.15454/08BX-VJ91; www.ibisba.fr), the French node of the European research infrastructure, EU-IBISBA (www.ibisba.eu).

References

[1] M.E. Himmel, S.-Y. Ding, D.K. Johnson, W.S. Adney, M.R. Nimlos, J.W. Brady, T.D. Foust, Biomass recalcitrance: Engineering plants and enzymes for biofuels production, Science 315(5813) (2007) 804-807.
[2] J.J. Bozell, G.R. Petersen, Technology development for the production of biobased products from biorefinery carbohydrates-the US Department of Energy's "Top 10" revisited, Green Chem. 12(4) (2010) 539-554.
[3] R. Kumar, S. Singh, O.V. Singh, Bioconversion of lignocellulosic biomass: biochemical and molecular perspectives, Journal of Industrial Microbiology and Biotechnology 35(5) (2008) 377-391.
[4] A. Villares, C. Moreau, C. Bennati-Granier, S. Garajova, L. Foucat, X. Falourd, B. Saake, J.G. Berrin, B. Cathala, Lytic polysaccharide monooxygenases disrupt the cellulose fibers structure, Sci Rep 7 (2017) 40262.
[5] C. Moreau, S. Tapin-Lingua, S. Grisel, I. Gimbert, S. Le Gall, V. Meyer, M. Petit-Conil, J.G. Berrin, B. Cathala, A. Villares, Lytic polysaccharide monooxygenases (LPMOs) facilitate cellulose nanofibrils production, Biotechnol. Biofuels 12 (2019).
[6] E. Drula, M.L. Garron, S. Dogan, V. Lombard, B. Henrissat, N. Terrapon, The carbohydrate-active enzyme database: functions and literature, Nucleic acids research 50(D1) (2022) D571-D577.
[7] T.M. Vandhana, J.L. Reyre, D. Sushmaa, J.G. Berrin, B. Bissaro, J. Madhuprakash, On the expansion of biological functions of lytic polysaccharide monooxygenases, The New phytologist 233(6) (2022) 2380-2396.
[8] M. Couturier, S. Ladeveze, G. Sulzenbacher, L. Ciano, M. Fanuel, C. Moreau, A. Villares, B. Cathala, F. Chaspoul, K.E. Frandsen, A. Labourel, I. Herpoel-Gimbert, S. Grisel, M. Haon, N. Lenfant, H. Rogniaux, D. Ropartz, G.J. Davies, M.N. Rosso, P.H. Walton, B. Henrissat, J.G. Berrin, Lytic xylan oxidases from wood-decay fungi unlock biomass degradation, Nat. Chem. Biol. 14(3) (2018) 306-+.
[9] J.W. Agger, T. Isaksen, A. Varnai, S. Vidal-Melgosa, W.G.T. Willats, R. Ludwig, S.J. Horn, V.G.H. Eijsink, B. Westereng, Discovery of LPMO activity on hemicelluloses shows the importance of oxidative processes in plant cell wall degradation, Proceedings of the National Academy of Sciences of the United States of America 111(17) (2014) 6287-6292.
[10] M. Couturier, N. Tangthirasunun, X. Ning, S. Brun, V. Gautier, C. Bennati-Granier, P. Silar, J.G. Berrin, Plant biomass degrading ability of the coprophilic ascomycete fungus Podospora anserina, Biotechnology Advances 34(5) (2016) 976-983.
[11] Y. Mathieu, O. Raji, A. Bellemare, M. Di Falco, T.T.M. Nguyen, A.H. Viborg, A. Tsang, E. Master, H. Brumer, Functional characterization of fungal lytic polysaccharide monooxygenases for cellulose surface oxidation, Biotechnology for Biofuels and Bioproducts 16(1) (2023) 132.
[12] M. Chemin, K. Kansou, K. Cahier, M. Grellier, S. Grisel, B. Novales, C. Moreau, A. Villares, J.G. Berrin, B. Cathala, Optimized Lytic Polysaccharide Monooxygenase Action

Increases Fiber Accessibility and Fibrillation by Releasing Tension Stress in Cellulose Cotton Fibers, Biomacromolecules 24(7) (2023) 3246–3255.
[13] K.H. Gardner, J. Blackwell, Structure of native cellulose, Biopolymers 13(10) (1974) 1975-2001.
[14] S.Y. Oh, D.I. Yoo, Y. Shin, H.C. Kim, H.Y. Kim, Y.S. Chung, W.H. Park, J.H. Youk, Crystalline structure analysis of cellulose treated with sodium hydroxide and carbon dioxide by means of X-ray diffraction and FTIR spectroscopy, Carbohydr. Res. 340(15) (2005) 2376-2391.
[15] M. Wada, Y. Nishiyama, P. Langan, X-ray structure of ammonia-cellulose I: New insights into the conversion of cellulose I to cellulose III, Macromolecules 39(8) (2006) 2947-2952.
[16] F.G. Støpamo, I. Sulaeva, D. Budischowsky, J. Rahikainen, K. Marjamaa, A. Potthast, K. Kruus, V.G.H. Eijsink, A. Várnai, Oxidation of cellulose fibers using LPMOs with varying allomorphic substrate preferences, oxidative regioselectivities, and domain structures, Carbohydr. Polym. 330 (2024) 121816.
[17] C. Bennati-Granier, S. Garajova, C. Champion, S. Grisel, M. Haon, S. Zhou, M. Fanuel, D. Ropartz, H. Rogniaux, I. Gimbert, E. Record, J.-G. Berrin, Substrate specificity and regioselectivity of fungal AA9 lytic polysaccharide monooxygenases secreted by *Podospora anserina*, Biotechnol. Biofuels 8 (2015) 90.
[18] C. Filiatrault-Chastel, D. Navarro, M. Haon, S. Grisel, I. Herpoël-Gimbert, D. Chevret, M. Fanuel, B. Henrissat, S. Heiss-Blanquet, A. Margeot, J.-G. Berrin, AA16, a new lytic polysaccharide monooxygenase family identified in fungal secretomes, Biotechnol. Biofuels 12(1) (2019) 55.
[19] W.P. Flauzino Neto, J.-L. Putaux, M. Mariano, Y. Ogawa, H. Otaguro, D. Pasquini, A. Dufresne, Comprehensive morphological and structural investigation of cellulose I and II nanocrystals prepared by sulphuric acid hydrolysis, RSC Advances 6(79) (2016) 76017-76027.
[20] P.K. Chidambareswaran, S. Sreenivasan, N.B. Patil, H.T. Lokhande, S.R. Shukla, Fine structural changes in native and mercerized fibrous cellulose brought about by ethylenediamine and methyl alcohol, J. Appl. Polym. Sci. 22(11) (1978) 3089-3099.
[21] T.M. Wood, Preparation of crystalline, amorphous, and dyed cellulase substrates, Methods in Enzymology, Academic Press1988, pp. 19-25.
[22] C. Moreau, X. Falourd, M. Talantikite, B. Cathala, A. Villares, Bifunctionalization of Cellulose Fibers by One-Step Williamson's Etherification to Obtain Modified Microfibrillated Cellulose, ACS Sustainable Chemistry & Engineering 10(40) (2022) 13415-13423.
[23] C. Hoebler, J.L. Barry, A. David, J. Delortlaval, Rapid acid hydrolysis of plant cell wall polysaccharides and simplified quantitative determination of their neutral monosaccharides by gas-liquid chromatography, J. Agric. Food Chem. 37(2) (1989) 360-367.
[24] B. Quéméner, D. Bertrand, I. Marty, M. Causse, M. Lahaye, Fast data preprocessing for chromatographic fingerprints of tomato cell wall polysaccharides using chemometric methods, J. Chromatogr. A 1141(1) (2007) 41-49.
[25] L. Segal, J.J. Creely, A.E. Martin, C.M. Conrad, An Empirical Method for Estimating the Degree of Crystallinity of Native Cellulose Using the X-Ray Diffractometer, Text. Res. J. 29(10) (1959) 786-794.
[26] B.J.C. Duchemin, Mercerisation of cellulose in aqueous NaOH at low concentrations, Green Chem. 17(7) (2015) 3941-3947.
[27] M. Schwanninger, J.C. Rodrigues, H. Pereira, B. Hinterstoisser, Effects of short-time vibratory ball milling on the shape of FT-IR spectra of wood and cellulose, Vib. Spectrosc. 36(1) (2004) 23-40.

[28] Y. Marechal, H. Chanzy, The hydrogen bond network in I-beta cellulose as observed by infrared spectrometry, Journal of Molecular Structure 523 (2000) 183-196.
[29] P.K. Chidambareswaran, S. Sreenivasan, N.B. Patil, H.T. Lokhande, Further studies on cellulose III polymorphs. Transformations to cellulose IV lattices and subsequent reactions, J. Appl. Polym. Sci. 27(2) (1982) 709-730.
[30] A.D. French, Idealized powder diffraction patterns for cellulose polymorphs, Cellulose 21(2) (2014) 885-896.
[31] J. Gong, J. Li, J. Xu, Z. Xiang, L. Mo, Research on cellulose nanocrystals produced from cellulose sources with various polymorphs, RSC Advances 7(53) (2017) 33486-33493.
[32] I. Sulaeva, D. Budischowsky, J. Rahikainen, K. Marjamaa, F.G. Støpamo, H. Khaliliyan, I. Melikhov, T. Rosenau, K. Kruus, A. Várnai, V.G.H. Eijsink, A. Potthast, A novel approach to analyze the impact of lytic polysaccharide monooxygenases (LPMOs) on cellulosic fibres, Carbohydr. Polym. 328 (2024) 121696.
[33] E.J. Foster, R.J. Moon, U.P. Agarwal, M.J. Bortner, J. Bras, S. Camarero-Espinosa, K.J. Chan, M.J.D. Clift, E.D. Cranston, S.J. Eichhorn, D.M. Fox, W.Y. Hamad, L. Heux, B. Jean, M. Korey, W. Nieh, K.J. Ong, M.S. Reid, S. Renneckar, R. Roberts, J.A. Shatkin, J. Simonsen, K. Stinson-Bagby, N. Wanasekara, J. Youngblood, Current characterization methods for cellulose nanomaterials, Chem. Soc. Rev. 47(8) (2018) 2609-2679.
[34] M.N. Muraleedharan, A. Karnaouri, M. Piatkova, M.-X. Ruiz-Caldas, L. Matsakas, B. Liu, U. Rova, P. Christakopoulos, A.P. Mathew, Isolation and modification of nano-scale cellulose from organosolv-treated birch through the synergistic activity of LPMO and endoglucanases, Int. J. Biol. Macromol. 183 (2021) 101-109.
[35] L. Solhi, J. Li, J. Li, N.M.I. Heyns, H. Brumer, Oxidative enzyme activation of cellulose substrates for surface modification, Green Chem. 24(10) (2022) 4026-4040.
[36] S. Koskela, S. Wang, P.M.P. Fowler, F. Tan, Q. Zhou, Structure and Self-Assembly of Lytic Polysaccharide Monooxygenase-Oxidized Cellulose Nanocrystals, ACS Sustainable Chemistry & Engineering 9(34) (2021) 11331-11341.
[37] S.L. Navarro, M. Tolgo, L. Olsson, T. Nypelo, Carboxylation of sulfated cellulose nanocrystals by family AA9 lytic polysaccharide monooxygenases, Cellulose (2023).
[38] A. Karnaouri, B. Jalvo, P. Moritz, L. Matsakas, U. Rova, O. Höfft, G. Sourkouni, W. Maus-Friedrichs, A.P. Mathew, P. Christakopoulos, Lytic Polysaccharide Monooxygenase-Assisted Preparation of Oxidized-Cellulose Nanocrystals with a High Carboxyl Content from the Tunic of Marine Invertebrate Ciona intestinalis, ACS Sustainable Chemistry & Engineering 8(50) (2020) 18400-18412.
[39] D. Cannella, N. Weiss, C.R. Hsieh, S. Magri, M. Zarattini, J. Kuska, N. Karuna, L.G. Thygesen, I. Polikarpov, C. Felby, T. Jeoh, H. Jorgensen, LPMO-mediated oxidation increases cellulose wettability, surface water retention and hydrolysis yield at high dry matter, Cellulose 30 (2023) 6259–6272.
[40] B. Song, B. Li, X. Wang, W. Shen, S. Park, C. Collings, A. Feng, S.J. Smith, J.D. Walton, S.-Y. Ding, Real-time imaging reveals that lytic polysaccharide monooxygenase promotes cellulase activity by increasing cellulose accessibility, Biotechnol. Biofuels 11(1) (2018) 41.
[41] S.K. Mudedla, M. Vuorte, E. Veijola, K. Marjamaa, A. Koivula, M.B. Linder, S. Arola, M. Sammalkorpi, Effect of oxidation on cellulose and water structure: a molecular dynamics simulation study, Cellulose 28 (2021) 3917-3933.
[42] F.T.F. Gomide, A.S. da Silva, E.P.D. Bon, T.L.M. Alves, Modification of microcrystalline cellulose structural properties by ball-milling and ionic liquid treatments and their correlation to enzymatic hydrolysis rate and yield, Cellulose 26(12) (2019) 7323-7335.

[43] A. Mittal, R. Katahira, M.E. Himmel, D.K. Johnson, Effects of alkaline or liquid-ammonia treatment on crystalline cellulose: changes in crystalline structure and effects on enzymatic digestibility, Biotechnol. Biofuels 4 (2011).
[44] D. Ciolacu, S. Gorgieva, D. Tampu, V. Kokol, Enzymatic hydrolysis of different allomorphic forms of microcrystalline cellulose, Cellulose 18(6) (2011) 1527-1541.
[45] X.D. Chen, L. Xiong, H.L. Li, L.Q. Zhang, G. Yuan, X.F. Chen, C. Wang, X.D. Chen, The inhibitory effect of xylan on enzymatic hydrolysis of cellulose is dependent on cellulose ultrastructure, Cellulose 27(8) (2020) 4417-4428.
[46] D. Ciolacu, L. Pitol, F. Ciolacu, Studies concerning the accessibility of different allomorphic forms of cellulose, Cellulose 19(1) (2012) 55-68.
[47] J. Hu, D. Tian, S. Renneckar, J.N. Saddler, Enzyme mediated nanofibrillation of cellulose by the synergistic actions of an endoglucanase, lytic polysaccharide monooxygenase (LPMO) and xylanase, Sci Rep 8(1) (2018) 3195.

Declaration of interests

☐The authors declare that they have no known competing financial interests or personal relationships that could have appeared to influence the work reported in this paper.

☒The authors declare the following financial interests/personal relationships which may be considered as potential competing interests:

Jean-Guy Berrin reports financial support was provided by Carnot 3BCar Institute. If there are other authors, they declare that they have no known competing financial interests or personal relationships that could have appeared to influence the work reported in this paper.

Highlights

- We studied two LPMOs from *Podospora anserine: Pa*LPMO9E and *Pa*LPMO9H.
- LPMOs are active on cellulose allomorphs I, II, III and on amorphous cellulose.
- *Pa*LPMO9H seemed more active than *Pa*LPMO9E, especially on cellulose I.
- LPMO action increases the accessibility to chemicals.